LA-UR-73-721

Conf-730442--2

LATE-TIME PHENOMENOLOGY PREDICTIONS WITH AN ALMOST-LAGRANGIAN CODE (U)*

J. U. Brackbill, C. D. Sutherland
M. S. Tierney
Los Alamos Scientific Laboratory
University of California
Los Alamos, New Mexico

May 11, 1973

*This work was performed under the joint auspices of the United States Atomic Energy Commission and the Defense Nuclear Agency (DNA Subtask No. HC-061, DNA Work Unit No. 15--Calculations at Low Altitude).

LATE-TIME PHENOMENOLOGY PREDICTIONS WITH AN ALMOST-LAGRANGIAN CODE (U)

J. U. Brackbill, C. D. Sutherland
M. S. Tierney
Los Alamos Scientific Laboratory
University of California
Los Alamos, New Mexico

ABSTRACT

An implicit, arbitrary Lagrangian-Eulerian technique recently developed at LASL has been extended to calculate the magnetohydrodynamic flow associated with a high altitude nuclear explosion. The present two-dimensional version of the code utilizing this technique offers two advantages with respect to existing, usually explicit phenomenology codes: (1) the almost-Lagrangian feature minimizes numerical diffusion and permits calculations of flows with high magnetic Reynolds numbers; (2) the implicit formulation circumvents the Alfvén problem and therefore makes possible the efficient calculation of low speed flows without the need for artificial limits on mass density, or fluid and signal speeds. The treatment of boundary conditions and zoning for an almost-Lagrangian calculation is discussed, and the solution technique for chemical rate equations is described.

INTRODUCTION

HANE calculations are performed to give predictions of persistent ionization in the earth's atmosphere between 80 and 400 kilometers altitude. Good predictions can be made only if the gross atmospheric motion and the convection of chemical species is accurately calculated.

The attainment of sufficient accuracy presents several difficulties, however, among them one whose fundamental source is the presence of the earth's magnetic field. Although the magnetic field does not energetically dominate the flow in the region of interest [1], it provides a mechanism for communicating disturbances over great distances. It is this action at a distance property, coupled with the essentially unbounded upward motion of the disturbance from the burst [2], which effectively enlarges the domain of dependence far beyond the region of interest. Thus, to correctly write the boundary conditions at the upper boundary of the region of interest,

one must calculate the disturbance of the magnetic field far above.

A second difficulty in the attainment of accuracy is in the calculation of the convection of chemical species. If the calculation is performed on a fixed Eulerian computation mesh, computational errors enhance the interdiffusion of chemical species. This often causes premature quenching of ionization.

In this paper, a computational method is proposed which solves both these difficulties by exploiting the properties of a variable resolution, semi-Lagrangian mesh. The applicability of the method to HANE problems is demonstrated by the results of two-dimensional, axisymmetric, single-fluid, MHD calculations with MHD-YAQUI detonation at 200 km altitude. (The computational method is an extension of the ICED-ALE method [3] to MHD [4].)

Variable resolution allows fine zoning in the region of interest, and crude zoning above in the region where connection with earth's magnetic field in vacuum is established. Thus the upper boundary conditions for the region of interest can be calculated at minimum extra expense. In part B of the Discussion section, the variable resolution mesh is described. In addition, the imposition of boundary conditions and stategies for computational efficiency are discussed. The semi or almost-Lagrangian mesh reduces computational diffusion by reducing the relative motion of the grid and fluid. Instead of solving the dynamical equations on an Eulerian mesh as has been done in the past, the equations are solved on a moving mesh composed of quadrilateral zones of arbitrary shape. The technique for doing this, the ALE algorithm [3], consists of two steps. In the first step, the dynamical equations are solved on a Lagrangian computation mesh. In the second step, the mesh is moved arbitrarily relative to the fluid. When almost-Lagrangian zoning is used, the computation mesh is adjusted in step two to more closely conform to an associated ideal mesh [4]. The adjustment of the mesh is made as small as is consistent with avoiding Lagrangian zoning difficulties so that the relative motion of the fluid and the mesh is minimized. Since computational diffusion arises out of truncation errors in the solution of convection terms, reducing the relative motion reduces diffusion. Most importantly, the almost-Lagrangian zoning reduces the interdiffusion of chemical species in the region of interest. The application of almost-Lagrangian zoning to HANE calculations is discussed in part A.

Finally, the computational method for the solution of chemical rate equations is outlined in part C. Other aspects of the computational method, such as the implicit formulation of the dynamical equations and the iteration technique used to solve them, are given elsewhere [3, 4]. They will not be discussed further here.

DISCUSSION

MHD-YAQUI solves the single component equations for magnetohydrodynamic flow in two dimensions. In axisymmetric problems, the magnetic field lies in the r-z plane. The equations of motion are integrated forward in time in discrete time steps which are chosen to satisfy certain stability and accuracy conditions. The data for each integration step, or cycle, is given at an array of points in the r-z plane. The points may be arbitrarily located relative to each other. Each data point at which kinetic variables, e.g., the position and velocity of a point in the fluid, are given is the vertex of a computation cell. The cells are formed by connecting neighboring vertices by straight lines to form a computation mesh of quadrilateral cells. At the center of each cell, thermodynamic variables, including the magnetic field components, are specified.

If the vertices were to move with the local fluid velocity, the mesh would simply be Lagrangian. It is the addition of a second step to the algorithm in which the vertex velocity may be specified in an arbitrary way that allows almost-Lagrangian zoning to be used. The calculation of the vertex velocities is discussed in the next part.

A. The Almost-Lagrangian Mesh

Since a complete description of the almost-Lagrangian method is available [4], this section will contain only a brief description of the method, and a discussion of some of the special problems encountered in its application to late-time HANE calculations.

Each computation cycle, a grid velocity is calculated at each vertex, which is the sum of the local fluid velocity and a small correction velocity. The small correction velocity is calculated to reduce the displacement of the computation mesh from an associated ideal mesh over a relaxation time τ. When the relaxation time is longer than the interval over which fluid velocities differ appreciably from zero, a reduction in the truncation errors in the convection terms is obtained. That is, while the local fluid velocity is non-zero, the mesh essentially follows the fluid. When the fluid velocity is once again small, the mesh slowly relaxes back to the associated ideal mesh over a relaxation time τ. In this way, the total motion between the mesh and fluid occurs over a longer time, and thus at a lower average rate, than it would in a comparable Eulerian calculation.

The ideal mesh used for the calculations presented here is nearly locally rectilinear and has the same distribution of vertices on the boundaries of the mesh as the computation mesh to which it is associated. At the end of each computation cycle, the components of the displacement of the computation

mesh from the associated ideal mesh are calculated from a pair of linear equations suggested by P. Browne at LASL. They are,

$$\delta r_o = \Sigma \left\{ \left(r_o - \tfrac{1}{2} (r_i + r_{i+1}) \right) / A_{i_{i+1}} \right\} / \Sigma (1/A_{i_{i+1}}), \qquad (1)$$

and

$$\delta z_o = \Sigma \left\{ \left(z_o - \tfrac{1}{2} (z_i + z_{i+1}) \right) / A_{i_{i+1}} \right\} / \Sigma (1/A_{i_{i+1}}), \qquad (2)$$

where r_i and z_i are the indices of the vertices neighboring vertex o, whose coordinates are (r_o, z_o), with i = 1, 2, 3, 4 (cyclic), and $A_{i_{i+1}}$ is given by,

$$A_{i_{i+1}} = \tfrac{1}{2} \left[(r_i - r_o) \quad (z_{i+1} - z_o) \; - \; (z_i - z_o) \; (r_{i+1} - r_o) \right].$$

From these displacements, a grid velocity is calculated from the equation,

$$\underset{\sim}{u}_g \; (\underset{\sim}{r}, t) = \underset{\sim}{u}_f \; (\underset{\sim}{r}, t) - \underset{\sim}{\delta} \; (\underset{\sim}{r}, t)/\tau, \qquad (3)$$

where $\underset{\sim}{u}_g$ is the grid velocity, $\underset{\sim}{u}_f$ the fluid velocity, $\underset{\sim}{\delta}$ the displacement of the computation mesh from the ideal mesh, and τ the relaxation time defined above. It is easily shown that reducing the displacements calculated from Eqs 1 and 2 makes the angles subtended by cell boundaries about each vertex more nearly right angles. Thus, repeated calculation of the grid velocities necessary to reduce these displacements relaxes the computation mesh toward a mesh with local rectilinearity. It should be noted that when the time step, δt, is twice τ the displacements are reduced to zero in one time step. However, τ is usually set to the largest value consistent with preventing excessive distortion of the computation mesh, and so $\delta t/\tau$

is usually so small that the reduction in the displacement each time step depends essentially linearly on δt. Thus, the relative motion over an interval of the order of τ will be nearly independent of the number of time steps in that interval.

The reduction of the displacements calculated from the equations above gives a desirable tendency to local rectilinearity in the computation mesh, but it does not solve all of the problems encountered in a HANE calculation. For example, although the prescription for local rectilinearity is global, the fluid flow may be quite local. This may cause the grid velocity to be larger than the fluid velocity in subregions of the mesh, thus actually increasing, rather than decreasing the computational diffusion, over a comparable Eulerian calculation. The solution to this problem is to limit the relative velocity between the fluid and the mesh to a fraction of the local fluid velocity. This can be done where the flow is either transient or shear free, as in the region below the burst where atmospheric heave occurs. Elsewhere, the relative velocity is not bounded in order that adjustments to the mesh to solve another problem can be made.

The other problem is that all rectilinear meshes are not equally desirable. For example, the mesh-boundary crossing condition on the time step makes very small zones undesirable because small zones mean small time steps. In addition, extremely elongated cells cause small time steps because of the explicit stability condition on viscous stress terms in the momentum equation. These undesirable meshes can be avoided by two strategies. First, vertices lying on the boundary can be moved so that they are equally spaced along the boundary. This would give a tendency for zones to become equal sized in the interior of the mesh. Second, a search can be made over the mesh for the smallest and for the most elongated cell in the mesh. When it is found, its size or shape can be adjusted to more nearly compare with that of its neighbors. Both of these strategies are employed in the calculations presented here, but only to the portion of the mesh lying above 1000 km altitude. Although the rate at which adjustments to cell sizes and shapes must be made is problem dependent the same rate works for calculations of 150 km and 200 km bursts. A more general approach to the problem would include constraints on zone sizes and elongations in the prescription for the associated ideal mesh.

An initial computation mesh for a 200 km burst calculation is shown in Fig. 1. The mesh's axis of symmetry lies on the left boundary. The mesh is divided into 21 zones radially and 37 zones axially. The zones range from 6 km in width and height to 60 km high by 100 km wide.

An almost-Lagrangian computation mesh for a 200 km burst calculation is shown in Fig. 2a at 10.0 seconds, and in Fig. 3a at 300.0 seconds problem time. A Lagrangian mesh is shown at the corresponding times in Figs. 2b and

3b. The Lagrangian mesh is constructed by moving the vertices of a fictitious mesh with the fluid, where the motion is found by bilinear interpolation on the almost-Lagrangian mesh. The differences between the two meshes in Fig. 2 are most pronounced in the first four or five columns to the right of the axis of symmetry, which lies on the left boundary of the mesh. This is the region over which the expanding disturbance has already swept, and in which the flow gradients are small. Here the effect of the mesh relaxer is most evident, because the adjustment, calculated from Eq 3, has been occurring over a long time compared with the passage time of the disturbance, since the relaxation time τ, is set to 10.0 seconds.

In Fig. 3, the top of the 25th zone of the Lagrangian mesh has risen to 3100 km altitude, marked by black dashes in Fig. 3, whereas the corresponding zone in the almost Lagrangian mesh has only risen to 2100 km. (The mesh above the 25th zone has been inactivated by a procedure which is outlined in part B.) The adjustment of the mesh,which makes zones similarly sized above 1000 km,is the primary reason for this difference. The differences below 1000 km, while evident,are less pronounced. However, this comparison indicates that the Lagrangian mesh is so well-behaved below 1000 km that a much longer relaxation time could have been used than 10 seconds, thus decreasing computational diffusion in the region of interest. Future calculations will be performed with a time dependent mesh relaxation time.

B. Top Boundary Treatment

At burst points above 100 km in the atmosphere, the atmospheric mass lying above the burst is insufficient to inertially contain the upward motion of heated air. Some of the momentum carried by this motion is transferred to the magnetic field to create disturbances which are then carried by means of the field back down into the region of interest. To illustrate this, Fig. 4 shows the magnetic field lines at 120 seconds after a detonation at 200 km. Note how the magnetic field lines below 1000 km altitude are held out by the bowing out of field lines above 1000 km. In addition, the unconfined upward motion of heated air results in a growing region of disturbance. In the calculations presented here, these problems are addressed by using a large initial mesh, and by allowing the top boundary of the mesh to move with the fluid. The boundary conditions on the free, Lagrangian boundary will now be discussed.

Consider the general specification of boundary conditions. The boundary conditions for YAQUI are homogeneous [3]. They are completely specified when the boundary velocities are determined. (In the case of magnetohydrodynamic calculations, the conductivity of the boundary and the orientation of the field at the boundary determine the velocity boundary conditions.) If one were to choose to make a line of constant i or constant j interior to the limits of the computation mesh a boundary, say a boundary between immiscible fluids, the

boundary conditions on the velocity components are specified as a function of time by the equation of motion. If, instead, this interior boundary were the boundary between the disturbed and undisturbed fluid, the stress which appears in the momentum equation is specified on the disturbed side by the calculation, and the undisturbed side by the initial conditions. Thus, if the ambient magnetic field, density, and pressure specified above the boundary are specified in a row of dummy cells, the equations of motion for the boundary vertices can be solved as they would be for an interior boundary. The independence of time of the magnetic field in the dummy cells imposes the boundary condition that the component of velocity normal to the ambient field is zero, for the change in direction of the magnetic field is given by,

$$\frac{d\underset{\sim}{B}}{dt} = \left|\underset{\sim}{B}\right| \frac{\partial \underset{\sim}{u}_{\perp}}{\partial \ell} \tag{4}$$

where $\underset{\sim}{B}$ is the magnetic field, $\underset{\sim}{u}_{\perp}$ the velocity perpendicular to $\underset{\sim}{B}$, and ℓ is the distance along the magnetic field line. Clearly, the assumption that the fluid motion should not change the field outside the boundary is valid if the fluid motion does not have sufficient kinetic energy to do so. The appropriate criterion for this is the Alfvén Mach number,

$$M_A = \tfrac{1}{2}\, \rho\, \underset{\sim}{u}^2/\underset{\sim}{B}^2/\mu,$$

where ρ is the mass density, $\underset{\sim}{u}$ the fluid velocity, and μ the permeability; which is the ratio of fluid kinetic energy to magnetic field energy. If M_A is small at the boundary, the assumption that ambient conditions prevail there is a reasonable one.

Of course magnetoacoustic or transverse Alfvén waves can propagate upstream through sub-Alfvén flow from the boundary to the interior of the mesh. However, the generation of important waves requires large disturbances in the flow. When the Alfvén Mach number of the outflow is of the order of one or less, errors in the outflow boundary conditions cannot create large disturbances. Thus the boundary will be sufficiently isolated from the region of interest even for sub-Alfvén flow.

In Fig. 5, the results of two calculations of a burst at 200 km are shown in which the height of the top boundary is varied. The plots on the left in these figures are for a calculation for which $M_A = 1.$ at the top

boundary, and those on the right for a calculation for which $M_A = 0.5$. In Figs. 5a and b, the magnetic field lines for the two calculations at 140.0 sec. show no disturbances propagating back from the boundary. In Figs. 5c and d, the iso-density contours are identical to within the resolution of the flow field, especially below 1000 km altitude.

A further saving in computation time can be obtained by deleting rows of zones at the top of the mesh when the condition,

$$\left| \frac{\partial u_\perp}{\partial \ell} \right| \tau < \varepsilon \,, \qquad (5)$$

is satisfied over the entire row, where ε is a small positive number, and τ is the grid relaxation time. By comparing Eqs. (5) and (4), one sees that this condition is equivalent to saying the flow has become time independent. In the results shown in Fig. 6 at 180.0 seconds, this procedure has eliminated 13 rows of zones out of 37 with ε equal to 10^{-4}, and τ equal to 10.0 seconds. The truncated mesh at an even later time, at 300 seconds, is shown in Fig. 3a. In Figs. 6a and b the magnetic field line plots, and in Figs. 6c and d, the density contours of a full and a truncated mesh are compared. It is obvious from these results that deleting zones has little effect on the results. It does, however, result in considerable savings in computation time. To integrate to 180 seconds with the full 21 x 37 zone mesh required 3896 cycles, whereas to integrate the truncated mesh to 180 seconds required 3004 cycles. Truncating the mesh reduces the time required to compute to 300 seconds problem time from 90 minutes to 60 minutes on a CDC 7600. Part of the reduction is due to reducing the size of the mesh.

C. Chemistry

In MHD-YAQUI, chemical species concentrations are stored at computation cell centers and species are convected from cell to cell just as the mass density is. Eight specie concentrations are stored, and interact through the following reactions.

(a) $N^+ + O_2 \longrightarrow NO^+ + O + 6.657\ eV$

(b) $O^+ + N_2 \longrightarrow NO^+ + N + 1.099\ eV$

(c) $NO^+ + e \rightleftharpoons N + O \quad (+2.76\ eV \longrightarrow)$

(d) $N + O_2 \rightleftharpoons NO + O \quad (+1.392\ eV \longrightarrow)$

(e) $N + NO \rightleftharpoons N_2 + O \quad (+3.252\ eV \longrightarrow)$

Reactions (a), (b) and (c) are the minimal set required to describe the relaxation of the ionization of the atmosphere at altitudes between 90 and 250 km. Reactions (d) and (e) have been included in an attemtp to describe the recombination of atomic neutrals into molecular neutrals. The rate constants for reactions (a), (b), and (d) and (e) are those given in the revised version of the DASA Reaction Rate Handbook (DASA 1948), while the rate constants for reaction (c) are [6]

$(\longrightarrow)$ $1.5 \times 10^{-4}/T$ cm^3/sec

$(\longleftarrow)$ $3.6 \times 10^{-12} \exp(-31{,}800/T)$ cm^3/sec.

T is the temperature in degrees Kelvin.

The rate equations corresponding to reactions (a) - (e) are solved numerically for the species concentrations in each hydrodynamics cell every third to fifth hydrodynamics cycle. Some fluxing of species between cells occurs between integrations of the rate equations, but usually over an interval less than 0.5 seconds. However, the rate equations are integrated over the full time interval spanned by the number of hydrodynamic cycles in which chemistry has been suppressed. This artifice usually reduces the computation time by a factor of three, and seems to introduce no significant error mainly because the fluxing of material from cell to cell is much smaller in the present, almost-Lagrangian numerical scheme than in a comparable Eulerian difference scheme.

Numerical integration of the rate equations is accomplished by a set of subroutines employing Gear's method [7]. In addition to the rate equations for the chemical species (nine of them), an equation describing the release of chemical energy is integrated. Provision has been made for adding an arbitrary fraction of the resulting energy accumulated over the chemical cycle to the interval energy of the cell (the so-called coupled chemistry). However, in the preliminary calculations presented in this paper, no chemical energy is returned to the hydrodynamics so that comparisons with the results of other codes using "uncoupled" chemistry on Lagrangian markers, may be made more easily. Future calculations will return energy liberated by chemical reactions to the fluid flow.

A final remark on the manner by which a temperature is computed for the assignment of rate constants is in order. The specified internal energy, I, of a cell is held constant during the chemistry integration cycle, and is equal to the value assigned by the last hydrodynamic computation cycle preceding the chemical integration. The temperature is

nevertheless allowed to vary according to

$$T = \frac{I}{k} \frac{\sum_{i=1}^{9} (\gamma_i - 1)\, m_i [n_i]}{\sum_{i=1}^{9} [n_i]}$$

where k is Boltzmann's constant, m_i and $[n_i]$ are respectively the particle mass and concentration for the i^{th} species and

γ_i = 5/3 for monatomic species,

= 7/5 for diatomic species.

CONCLUSION

Representative results for a 200 km burst are shown in Fig. 7. No comparison with other calculations is given here, because it has been found that the initial conditions differ, in several important respects, from those used by MRC and NRL. For example, the air is heated much more strongly by the initial condition generating code, ET2F1, than by, say, MODEL 2. This accounts for differences in the electron densities at later times, through the temperature dependence of reaction rates. One calculation of a 150 km burst with corrections to the initial conditions has been performed, and the results are reported elsewhere in these proceedings. [8]

REFERENCES

1. Yu. P. Raizer, "The deceleration and energy conversions of a plasma expanding in a vacuum in the presence of a magnetic field", NASA Tech. Trand. No. TTF-239 (1964).

2. Ya. B. Zel'dovich and Yu. P. Raizer, "Physics of Shock Waves and High-Temperature Hydrodynamic Phenomena", Vol. 2, Ch. 12 Academic Press, New York (1967).

3. A. A. Amsden and C. W. Hirt, "YAQUI: An Arbitrary Lagrangian-Eulerian Computer Program for Fluid Flows at All Speeds", Report No. 5100, Los Alamos Scientific Laboratory, Los Alamos, NM 1972.

4. J. U. Brackbill and W. E. Pracht, "An Implicit, Almost-Lagrangian Algorithm for Magnetohydrodynamics", submitted for publication to J. Comp. Phys.

5. J. Boris and K. Hain, "Late-Time HANE Calculations on Modern Computers", DNA HANE Symposium (SRD), Vol. 6, p. 165 (1971); Fredric E. Fajen, "The MICE Technique", (U) DNA HANE Symposium (SRD), Vol. 6, p. 121 (1971); Fredric E. Fajen, "MICE: An Implicit Difference Scheme for MHD Calculations", (U) MRC-R-12, Mission Research Corp., Santa Barbara, CA 93101 (1973).

6. Fredric E. Fajen and Dale Sappenfield, "Single-Burst Weapons Effects Calculations for Altitudes between 97 and 250 km.", (U), LA-4606, June 1971, p. 35 (S-FRD).

7. A. C. Hindmarsh, "GEAR": Ordinary Differential Equation System Solver", Lawrence Livermore Laboratory, University of California, UCID-30001, Rev. 1, August 1972.

8. J. U. Brackbill, C. D. Sutherland, M. S. Tierney, J. Zinn, "A Debris-Energy Patch Calculation" (S-FRD), DNA HANE Symposium, San Diego (1973).

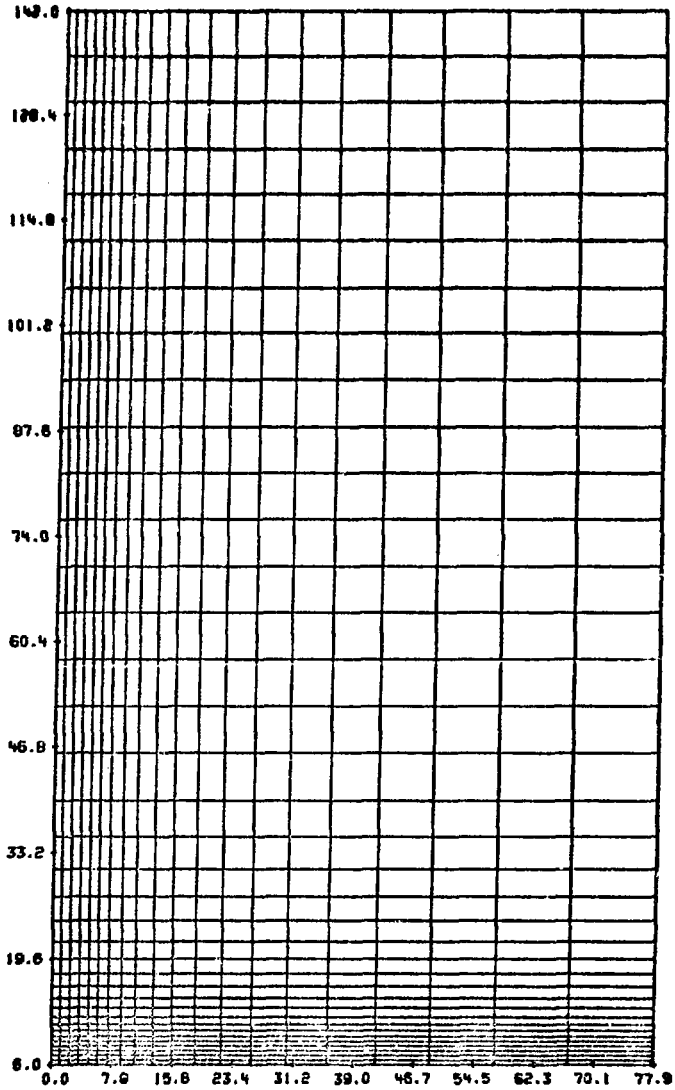

Fig. 1. The computation mesh at the initial time is shown. The mesh is subdivided into 21 radial zones and 37 axial zones, ranging from 6 to 60 km in height and 6 to 100 km in width.

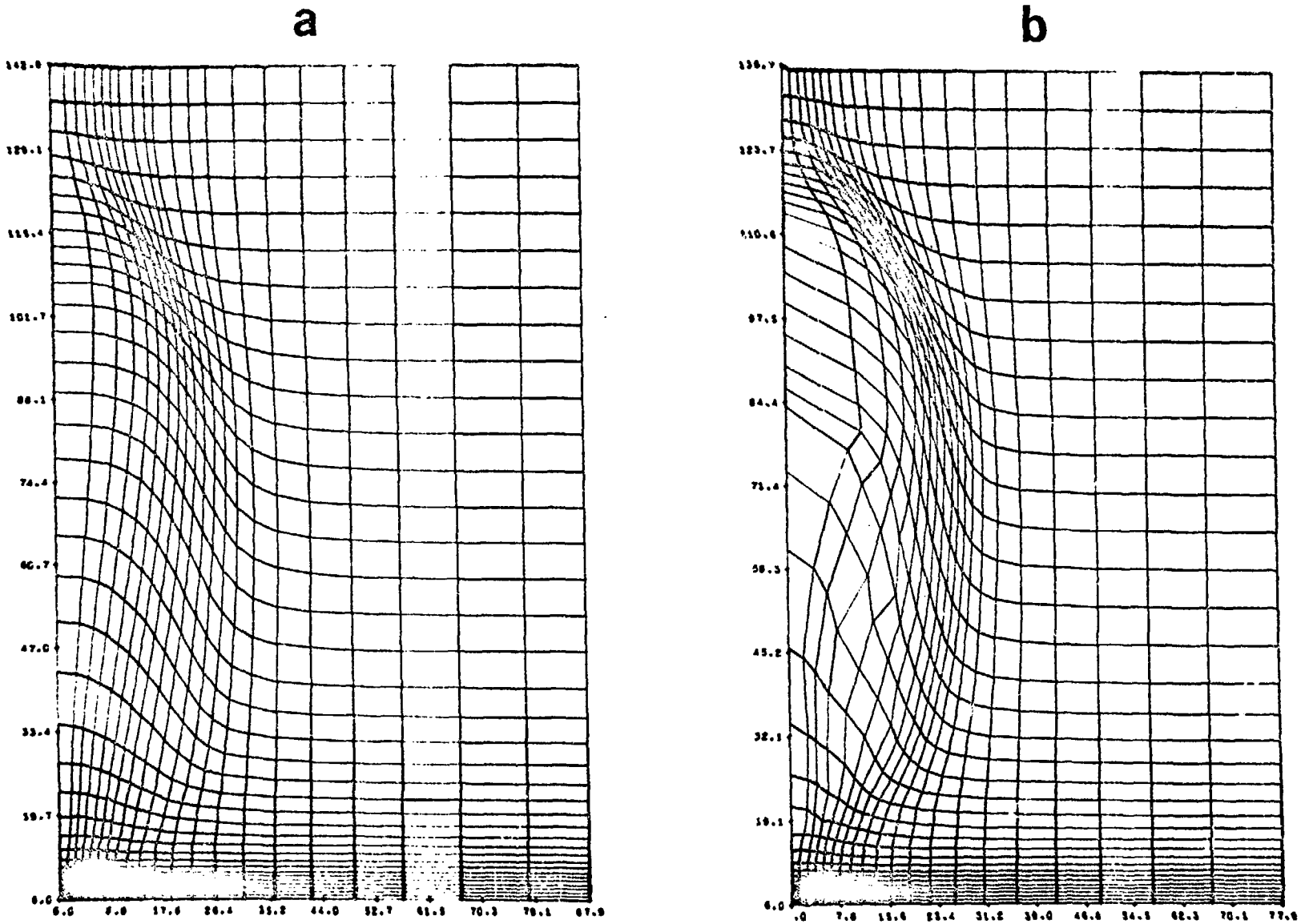

Fig. 2. An almost-Lagrangian and Lagrangian mesh at 10 sec. problem time are shown in Figs. 2a and 2b respectively. Units are tens of kilometers.

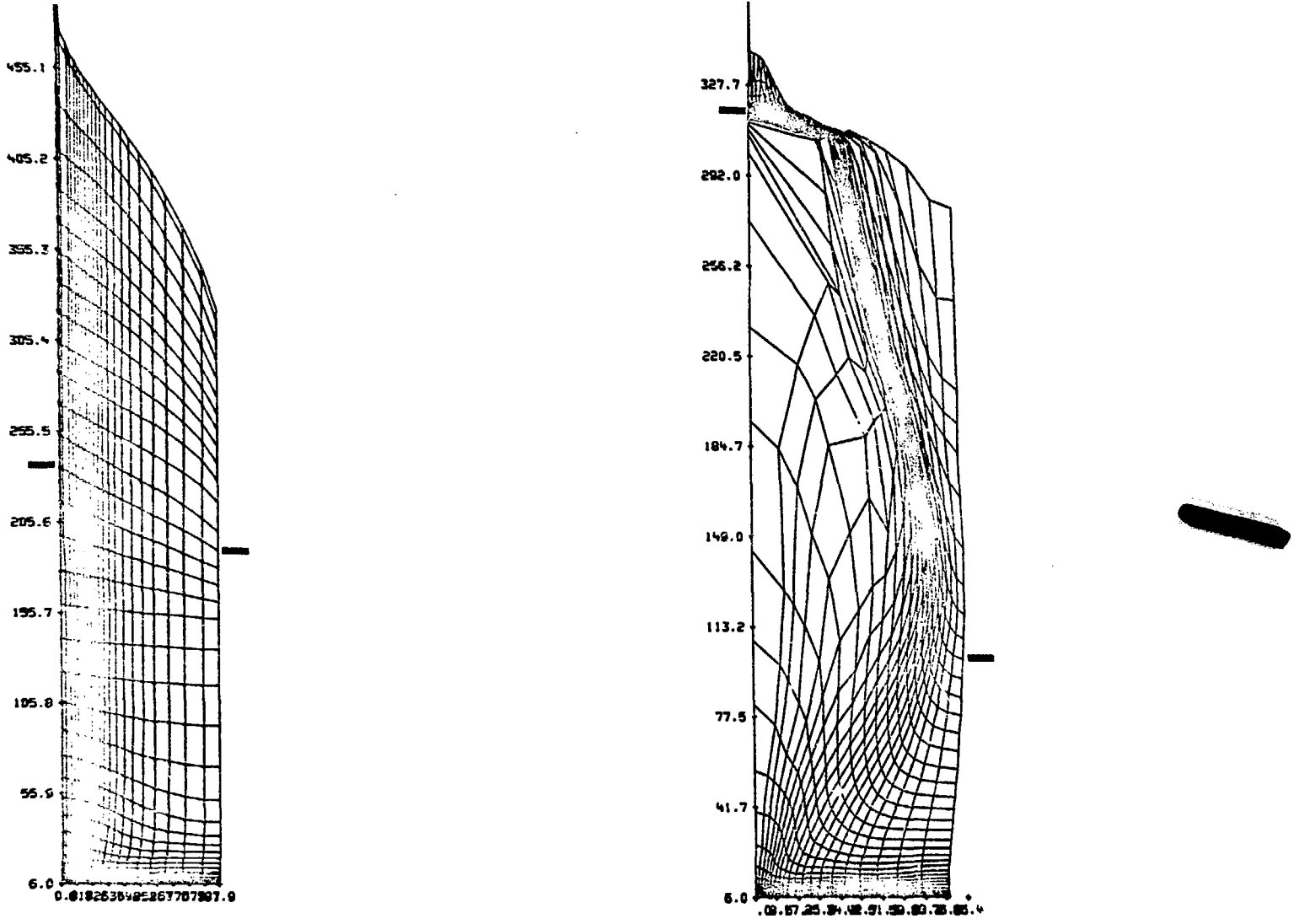

Fig. 3. An almost-Lagrangian and Lagrangian mesh are shown at 300 sec. problem time in Figs. 3a and 3b respectively. The black markers label the top zone of the active mesh.

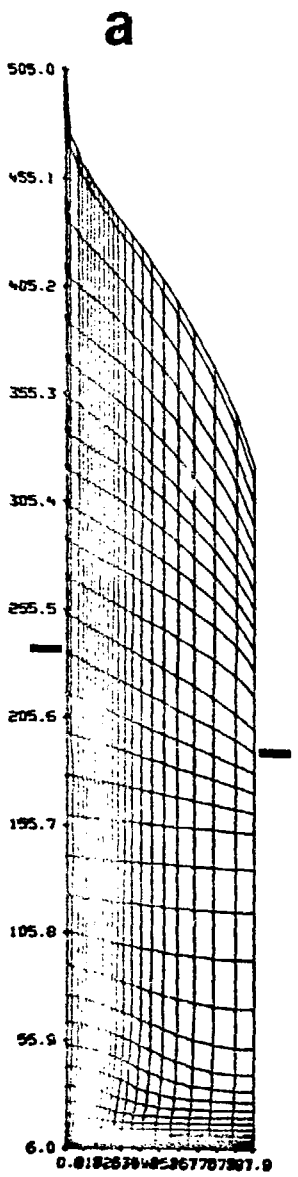
a
505.0
455.1
405.2
355.3
305.4
255.5
205.6
155.7
105.8
56.9
6.0

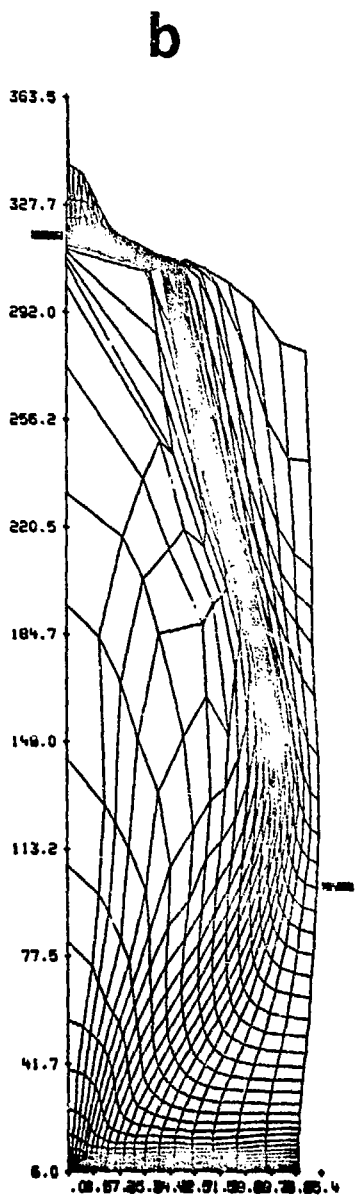
b
363.5
327.7
292.0
256.2
220.5
184.7
149.0
113.2
77.5
41.7
6.0

2

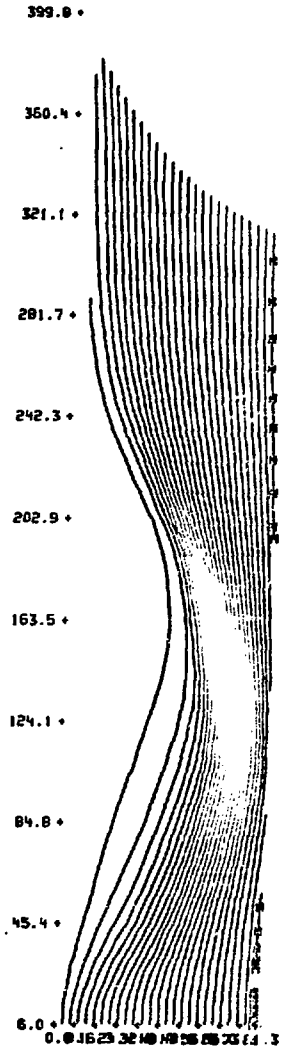

Fig. 4. The magnetic field lines at 120 seconds are shown for a burst at 200 km. The units are in tens of kilometers.

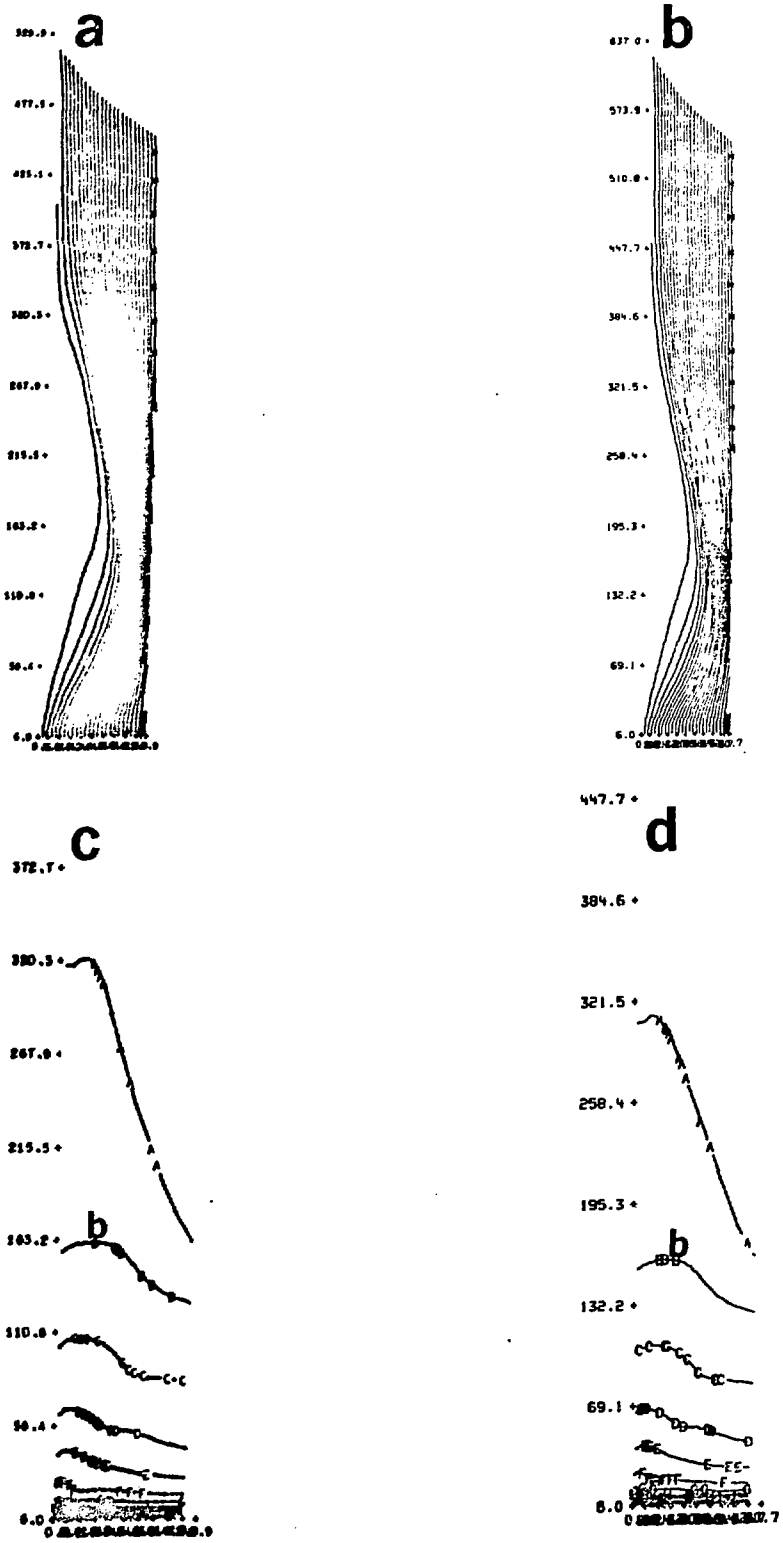

Fig. 5. A comparison between a calculation with M_A equal to one in Figs. 5a and 5c and one with M_A equal to one-half in Figs. 5b and 5d, is shown at 140 sec. The top two graphs are magnetic field lines, the bottom two iso-density contours. The iso-density contour labelled b represents a density of 10^{-13} g/cm^3.

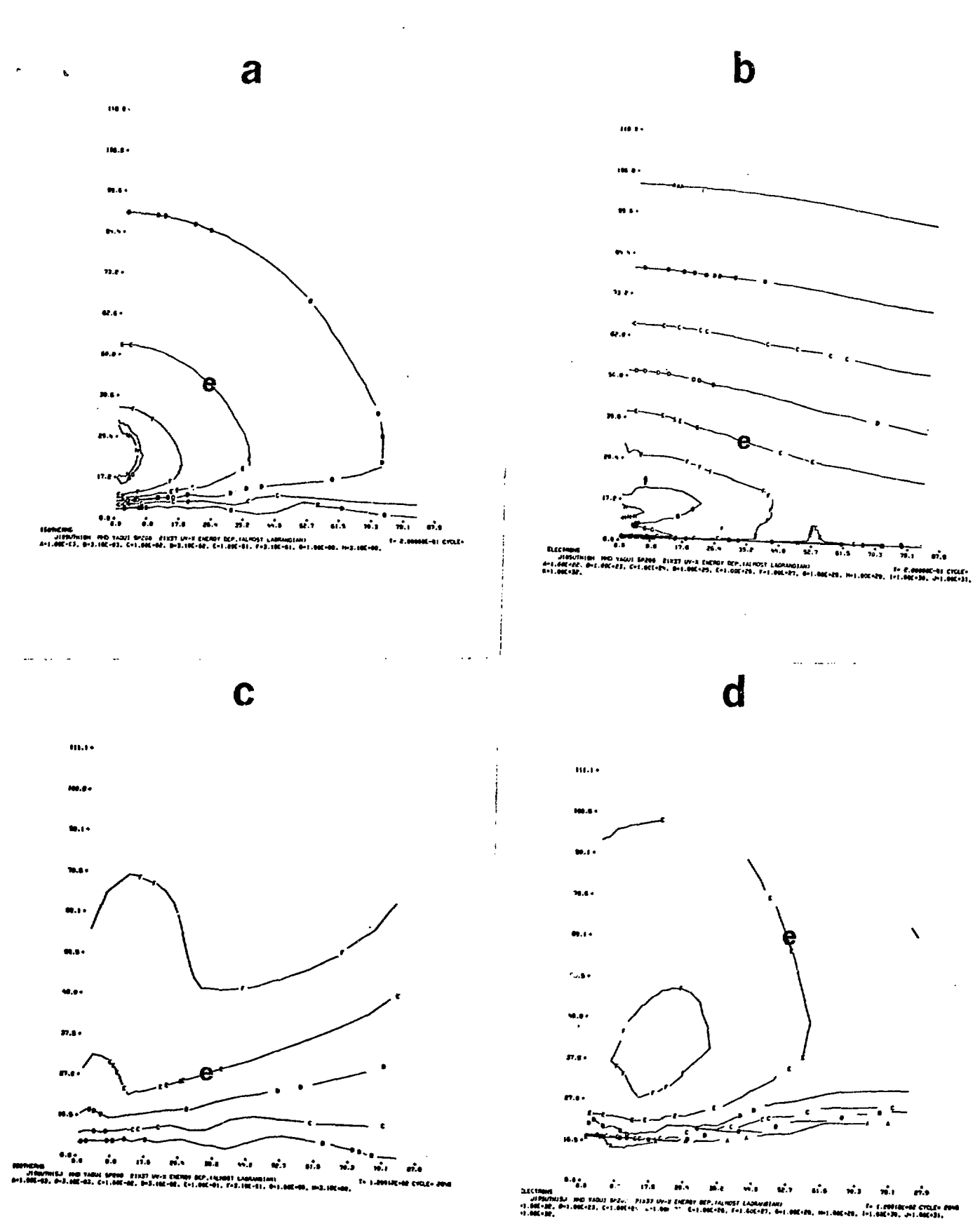

Fig. 7. Representative output from a calculation of a burst at 200 km is shown. In Fig. 7a and 7c, the iso-energy contours at 0 and 120 seconds are shown with the contour labelled e corresponding to 10^{11} g/cm^3. In Figs. 7b and 7d, electron density contours at 0 and 120 seconds are shown, with the contour labelled e corresponding to 10^8 electrons/cm^3.

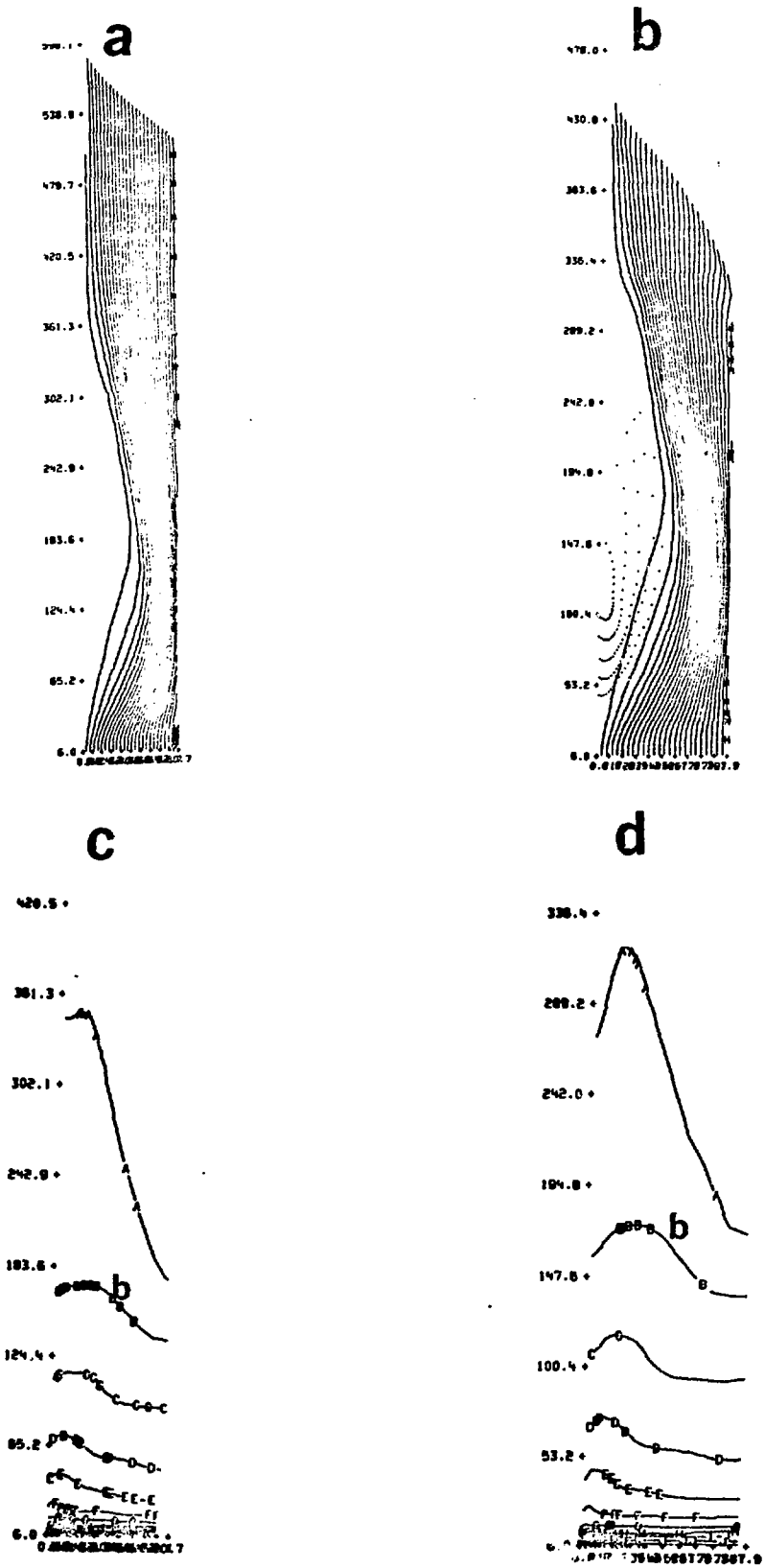

Fig. 6. A comparison between a calculation with a full mesh (M_A equal to one) in Figs. 6a and 6c, and a mesh from which zones have been deleted in Figs. 6b and 6d, is shown at 180 secs. The top two graphs are magnetic field lines, the bottom two iso-density contours. The iso-density contour labelled b represents a density of 10^{-13} g/cm^3.